Journal of the Optical Society of America B
OPTICAL PHYSICS

# Ultrathin flexible terahertz metamaterial bandstop filter based on laser-induced graphene

RONGXUAN ZHANG,[1] GUWEI ZONG,[1] SHUANGYUE WU,[1] RUIQI SONG,[1] XU ZHANG,[1] SHIJUN GE,[2] WEI HU,[2] LEI WANG,[1,2,3,*] AND YANQING LU[2]

[1] *College of Electronic and Optical Engineering, Nanjing University of Posts and Telecommunications, Nanjing 210023, China*
[2] *National Laboratory of Solid State Microstructures, College of Engineering and Applied Sciences, Key Laboratory of Intelligent Optical Sensing and Manipulation, Nanjing University, Nanjing 210093, China*
[3] *State Key Laboratory of Millimeter Waves, Southeast University, Nanjing, Jiangsu 210096, China*
**Corresponding author: wangl@njupt.edu.cn*

*Received 16 December 2021; revised 7 March 2022; accepted 7 March 2022; posted 8 March 2022; published 25 March 2022*

**An ultrathin, flexible metamaterial filter operated at terahertz (THz) frequencies based on one-step $CO_2$ laser-induced graphene (LIG) is proposed. The effects of laser machining parameters on conductivity and THz transmittance of the LIG are investigated, and a bandstop filter is fabricated from an ∼50 μm polyimide film using the LIG method with relatively high laser power and scanning speed. At a blocking central frequency of 0.67 THz, the planar filter transmission is ∼40% with only small variations for different bending angles. The simple, low-cost LIG method enables fabrication of THz metamaterial devices with great potential for THz imaging, sensing, and detection.**

https://doi.org/10.1364/JOSAB.451510

## 1. INTRODUCTION

Terahertz (THz) radiation in the frequency range of 0.1–10 THz has great potential in spectroscopy, biomedical technologies, and high-speed wireless communication [1–3]. There are still considerable challenges to develop high-efficiency and practical THz devices because most of the naturally available materials cannot be used due to their weak electric and magnetic responses in the THz region [4]. Metamaterials are artificial electromagnetic media composed of subwavelength periodic structures and are the most promising candidates for such devices because they allow THz wave manipulation through structural design [5,6]. Additionally, space-time metamaterials and metasurfaces [7,8] may also intrigue THz field manipulation effects. In recent years, diverse metamaterial filters have been proposed and widely used in imaging [9,10], sensing [11,12], and other applications. However, most conventional metamaterial filters are made of metal or silica, which are not flexible and incur high manufacturing cost for lithography, thereby limiting their application prospects.

Carbon-based materials, such as carbon nanotubes, graphene, and graphite, have garnered extensive attention owing to their tremendous rich functions and are used widely in applications requiring flexible electronics, such as strain sensors [13,14]. However, traditional chemical vapor deposition is complicated and difficult for forming patterned structures [15,16]. It is also difficult to ensure good combination during the transfer process and large-scale integration. Ivaškevičiūtė-Povilauskienė *et al.* reported the fabrication of THz zone plates with integrated cross-shaped filters using picosecond laser writing on thin graphite films; however, their processing cost remained high [17]. In 2014, Tour developed laser-induced porous graphene films from commercial polyimide (PI), which is the most promising material for flexible electronic substrates [18]; this fabrication method does not require conventional lithography techniques using masks and restricted operational conditions. Many applications have, hence, been proposed on the basis of this method, including sensors [19], electrodes [20,21], and microsupercapacitors [22–24]. In 2020, Wang *et al*. reported the fabrication of THz traditional gratings and Fresnel zone plates using 450 nm laser writing on PI film, which indicates that laser-induced carbon-based materials are promising candidates for THz devices [25]. However, to the best of our knowledge, carbon-based THz metamaterial devices using the laser-induced graphene (LIG) method have not been reported in literature.

Herein, we first demonstrate the relationship of laser machining parameters on the conductivity and THz transmittance of LIG. Then, the metamaterial filter, which consists of a subwavelength periodic array of graphene disks, is realized based on the optimized laser power and scanning speed. The experimental results show that the central frequency of the LIG-based metamaterial THz bandstop filter remains stable at 0.67 THz and only the transmittance varies with the bending angles.

## 2. FABRICATION AND CHARACTERIZATION

Figure 1 illustrates the fabrication process consisting of a $CO_2$ laser processing system with a focal spot size of 50 μm and

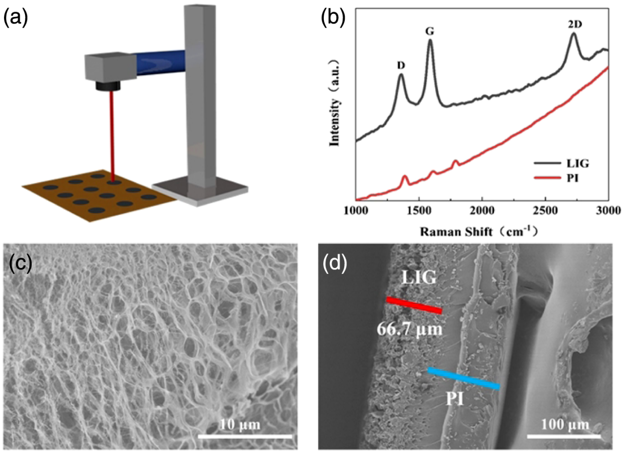

**Fig. 1.** (a) Schematic of LIG fabrication; (b) representative Raman spectra of the LIG and unprocessed PI; (c) SEM image of the fabricated LIG; (d) cross-sectional SEM image of the fabricated LIG.

wavelength of 10.6 µm. The power of the $CO_2$ laser is continuously tunable from 0.01 to 30 W. The laser scanning speed is varied from 1 to 1000 mm/s. With computer-controlled laser scribing, the LIG can be readily written in various geometries in the ambient environment. Raman spectroscopy and morphological characterization of the LIG samples were performed for comparison with the results of PI. The Raman spectrum of LIG (black curve) in Fig. 1(b) has three prominent peaks: the D peak at $\sim 1350\ \mathrm{cm}^{-1}$ from disorder-induced or bent sp2 carbon bonds, the G peak at $\sim 1580\ \mathrm{cm}^{-1}$ denoting the symmetry-allowed graphene band, and the 2D peak at $\sim 2700\ \mathrm{cm}^{-1}$ originating from second-order zone-boundary phonons. The Raman spectrum of the unprocessed PI film (red curve) does not exhibit these peaks. The laser power and scanning speed were set to 10 W and 260 mm/s, respectively. Figure 1(c) shows the scanning electron microscope (SEM) image of the LIG film. The randomly distributed microscale hollows appear to be induced by the rapid liberation of gaseous products. The cross-sectional SEM image of the LIG is shown in Fig. 1(d); the LIG is observed to have expanded to the outside; thus, the total thickness of the LIG (red line) and unprocessed PI (blue line) is more than 100 µm.

## 3. LASER POWER AND SCAN SPEED-DEPENDENT ELECTRICAL CONDUCTIVITY AND THZ TRANSMISSION

Because the insulating PI can be converted into conductive graphene, we further investigate the effects of the laser power and scanning speed on the DC electrical conductivity of the LIG using a four-point probe instrument. The laser scanning speed was set to 260 mm/s. Figure 2(a) shows that, when the laser power is low, i.e., from 6 to 8 W, the electrical conductivity remains almost zero. The threshold of the laser power for generating LIG is ~8 W. The electrical conductivity increases monotonically as the laser power increases from 8 to 12 W. This improvement in the LIG conductivity suggests that more graphene is generated with an increase in laser power. Above 12 W, the high laser power penetrates the sample that cannot be used. The dependence of the laser scanning speed on the electrical conductivities of the samples is compared, and the results corresponding to various laser powers are shown in Fig. 2(b). The conductivity generally decreases monotonically as the scan speed increases; this is because the heat accumulated on the PI is low when the scan speed is high, thereby generating less graphene. However, when the power is increased, more graphene is generated, and the conductivity recovers. The laser energy density Φ can be calculated as [25]

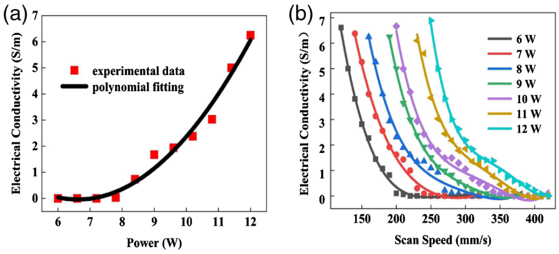

**Fig. 2.** (a) Laser-power-dependent electrical conductivity of the LIG for a laser scanning speed of 260 mm/s; (b) laser-scanning-speed-dependent electrical conductivity of the LIG at different laser powers.

$$\Phi = \frac{P}{V \times d}, \tag{1}$$

where $P$ is the laser power, $V$ is the scanning speed, and $d$ is the laser spot diameter; moreover, a high laser fluence corresponds to large electrical conductivity. It is worth noting that the low power and scanning speed of the laser are generally equivalent to high power and scanning speed from the formula above. Previous reports on the generation of graphene by laser action on PI have adopted low-power and low-speed processing methods. Although such processing methods are suitable for large-sized devices, they are unsuitable for processing small structures because a large amount of heat generated in the process of the LIG will cause the graphene units to expand outward, and adjacent structural units will be connected as a whole. The high-speed and high-power processing are more suitable for the fabrication of the THz metamaterials, which consist of subwavelength periodic structures. The parameters $P$ and $V$ work well within certain limits for certain PI films. However, there are optimal laser powers and scanning speeds for high-quality THz metamaterial LIG devices.

Next, THz time-domain spectroscopy (TAS7400SP; Advantest Corporation) was used to characterize the performances of the LIG films obtained using different laser parameters. Figure 3 shows the representative transmittance spectra of the LIG at different laser powers and scanning speeds. When the laser power is less than 6 W and the scan speed is greater than 260 mm/s, the transmission is similar to that of the unprocessed PI film, accompanied by high transmittance in the THz band; this indicates that the carbonization of PI films has not yet occurred. As the power gradually increases from 6 to 12 W, the THz transmission gradually decreases for a given scanning speed. The curved plane (blue) of the high scanning speed is above that of the low scanning speed, which indicates that the transmission is higher with greater scan speeds for a given laser power. The black plane clearly shows that when the laser power is 10 W, the transmission is nearly zero from 0.5 to 1.5 THz at

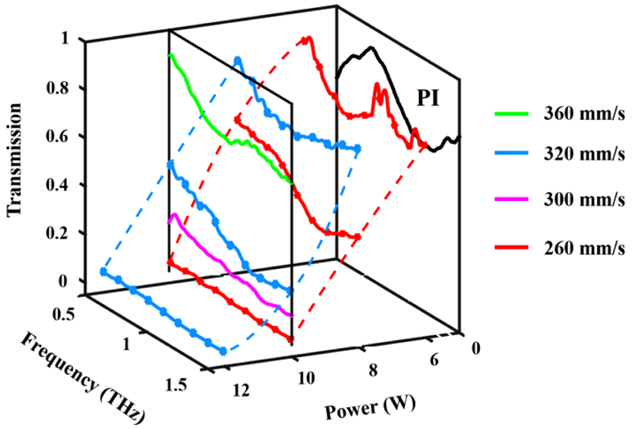

**Fig. 3.** THz transmission of the LIG film and its dependency on the tunable laser power and scanning speed.

a scan speed of 260 mm/s; in this case, the reflections are nearly zero or very low and are not shown. This is attributable to the porous microstructure of the LIG, as shown in Fig. 1(c), which greatly enhances the antireflectance capability.

## 4. THz METAMATERIAL FILTER AND DISCUSSION

The characteristics of the THz metamaterial bandstop filter based on LIG were investigated next. Figure 4(a) shows the schematic of the proposed graphene metamaterial THz filter, which is symmetric. The linearly polarized THz wave is incident normally with the electric field E along the $x$ axis (or the $y$ axis) direction. The filter is composed of a single layer of a graphene disk array, which is fabricated on a PI film of thickness approximately 50 μm. To ensure that the generated LIG metamaterial is of high quality, the optimized laser power and scanning speed of 10 W and 300 mm/s, respectively, were used. Figure 4(b) shows an image of the graphene metamaterial as seen under an optical microscope, where the radius of the disk is $r = 100$ μm and period of the filter is $P = 320$ μm. It is observed that the black area in Fig. 4(b) is carbonized to generate graphene. The small asymmetry in the disk and period due to the LIG method has little effect on the transmission spectra of the filter. The PI spacer is considered as a lossy material with a dielectric constant of $\varepsilon = 3.23$ and dielectric loss tangent of $\tan\delta = 0.0334$. A commercial electromagnetic solver (CST Microwave Studio 2018) was used for the simulations. The equivalent electrical conductivity of LIG is set to 0.6 S/m. The thickness of the graphene disk array is set to 50 μm as our LIG in the metamaterial filter experimentally has a thickness of about 50 μm and expands to the outside from the PI film, which can be seen from the cross-sectional SEM image of the LIG. The typical bandstop frequency selection effect can be observed in the transmission of the metamaterial LIG between 0.3 and 0.8 THz. The experimental result (black line) shown in Fig. 4(c) indicates that the modulation depth reaches 63% at a frequency of 0.67 THz, which is slightly different from the simulated result (red line). This difference may be caused by the fabrication, measurement, and simulation tolerances. The filter's −3 dB bandwidth is ∼0.11 THz, and the Q value is 6.09. The simulated THz electric field distribution of the metamaterial filter at 0.67 THz is shown in Fig. 4(d); hotspots are observed at the rim of the graphene disks at the resonance frequency on which biological samples can be placed for detection.

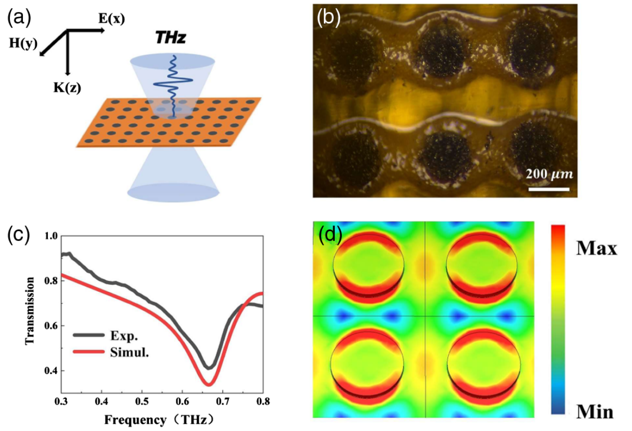

**Fig. 4.** (a) Schematic of the proposed THz metamaterial filter consisting of the graphene disk array; (b) image of the graphene metamaterial under an optical microscope; (c) transmission spectra of the filter: simulated (red line) and experimental (black line) results; (d) simulated THz electric field hotspot distribution of the filter at a resonance frequency of 0.67 THz.

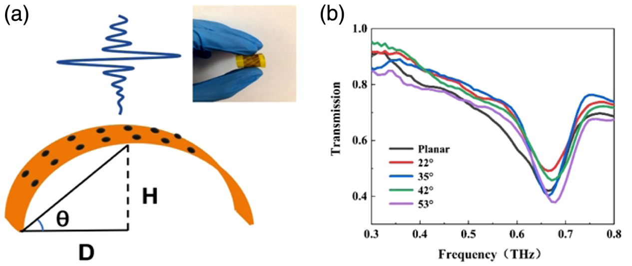

**Fig. 5.** (a) Schematic illustration of the flexible THz metamaterial filter; inset, photograph of the fabricated flexible THz filter; (b) transmission spectra of the filter for different bending angles.

Owing to the small thickness of the PI film, the filter has good mechanical flexibility. To gain further insights into the flexible THz characteristics, the filter was bent to form a curved surface for measurement. As shown in Fig. 5(a), $\theta$ is the bending angle of the flexible filter, $H$ is the height from the top of the arc to the test bench, and $D$ is the distance between the highest point of the arc to the edge of the sample along the test bench. When $D$ and $H$ are 11 and 7.8 mm, respectively, $\tan\theta = 0.709$ such that the bending angle is 35°. The transmittances of the filter in the planar state and at different bending angles are shown in Fig. 5(b). There are slight differences in the transmissions among all the bending angles, and no remarkable resonance frequency shifts are observed.

Unlike previously reported LIG devices, the unit of the proposed LIG metamaterial is smaller in size and more suited for flexible THz metamaterials. The properties of the unit can also be adjusted easily by tuning the laser processing parameters to change the graphene morphology, thereby changing the THz characteristics of the LIG device. In addition, LIG has excellent photothermal conversion capacity, high thermal conductivity, good thermal stability, and porous structure, which can be used to add microparticles, thus making it a promising candidate for THz applications. However, this technology is still in its infancy; owing to the limited wavelength of the $CO_2$ laser, the resolution of the metamaterial unit is a little poor. The precision and performance of the LIG THz metamaterial device are, therefore, available for further improvement. The structural properties can be optimized by a more precise laser machining system or doping metal nanoparticles in the porous structures of the LIG devices. In addition, temporally modulated THz metamaterials based on LIG are worth studying [26].

## 5. CONCLUSION

In summary, we propose an ultrathin flexible THz metamaterial bandstop filter fabricated by one-step LIG using a PI film. Based on different laser powers and scanning speeds, the conductivity and THz transmittance of the LIG are easily adjusted. A prototype filter was fabricated using optimized laser machining parameters, with the modulation depth attenuated to ~40% at 0.67 THz. The experimental results agreed well with numerical simulations. Furthermore, the central resonance frequency remained stable for different bending angles, which indicates that the proposed filter is not only suitable for planar but also curved geometries. The LIG method, thus, offers a one-step, large-area, and fast approach without masks for fabricating cost-effective, reliable, and flexible carbon-based metamaterial THz devices, which are expected to be applicable to various purposes, ranging from THz communication to THz biological detection and sensing in the near future.

**Funding.** Natural Science Foundation of Jiangsu Province (BK20211277); China Postdoctoral Science Foundation (2019M651768, 2020T130285); Natural Science Foundation of Jiangsu Province, Major Project (BK20212004); Fundamental Research Funds for the Central Universities (021314380095); State Key Laboratory of Millimeter Waves (K202226).

**Acknowledgment.** We thank the National Laboratory of Solid State Microstructures for the use of their equipment.

**Disclosures.** The authors declare no conflicts of interest.

**Data availability.** Data underlying the results presented in this paper are not publicly available at this time but may be obtained from the authors upon reasonable request.

## REFERENCES

1. M. Tonouchi, "Cutting-edge terahertz technology," Nat. Photonics **1**, 97–105 (2007).
2. M. Hangyo, "Development and future prospects of terahertz technology," Jpn. J. Appl. Phys. **54**, 120101 (2015).
3. Y.-Y. Ji, F. Fan, S.-T. Xu, J.-P. Yu, Y. Liu, X.-H. Wang, and S.-J. Chang, "Terahertz dielectric anisotropy enhancement in dual-frequency liquid crystal induced by carbon nanotubes," Carbon **152**, 865–872 (2019).
4. X. C. Zhang, A. Shkurinov, and Y. Zhang, "Extreme terahertz science," Nat. Photonics **11**, 16–18 (2017).
5. Y. Ma, Q. Chen, J. Grant, S. C. Saha, A. Khalid, and D. R. S. Cumming, "A terahertz polarization insensitive dual band metamaterial absorber," Opt. Lett. **36**, 945–947 (2011).
6. K. V. Sreekanth, Y. Alapan, M. ElKabbash, E. Ilker, M. Hinczewski, U. A. Gurkan, A. De Luca, and G. Strangi, "Extreme sensitivity biosensing platform based on hyperbolic metamaterials," Nat. Mater. **15**, 621–627 (2016).
7. G. Castaldi, V. Pacheco-Peña, M. Moccia, N. Engheta, and V. Galdi, "Exploiting space-time duality in the synthesis of impedance transformers via temporal metamaterials," Nanophotonics **10**, 3687–3699 (2021).
8. X. Wang, V. S. Asadchy, S. Fan, and S. A. Tretyakov, "Space–time metasurfaces for power combining of waves," ACS Photon. **8**, 3034–3041 (2021).
9. T. Xu, Y.-K. Wu, X. Luo, and L. J. Guo, "Plasmonic nanoresonators for high-resolution colour filtering and spectral imaging," Nat. Commun. **1**, 59 (2010).
10. S. Yokogawa, S. P. Burgos, and H. A. Atwater, "Plasmonic color filters for CMOS image sensor applications," Nano Lett. **12**, 4349–4354 (2012).
11. J. F. O'Hara, R. Singh, I. Brener, E. Smirnova, J. Han, A. J. Taylor, and W. Zhang, "Thin-film sensing with planar terahertz metamaterials: sensitivity and limitations," Opt. Express **16**, 1786–1795 (2008).
12. Y.-T. Chang, Y.-C. Lai, C.-T. Li, C.-K. Chen, and T.-J. Yen, "A multi-functional plasmonic biosensor," Opt. Express **18**, 9561–9569 (2010).
13. D. J. Lipomi, M. Vosgueritchian, B. C. Tee, S. L. Hellstrom, J. A. Lee, C. H. Fox, and Z. Bao, "Skin-like pressure and strain sensors based on transparent elastic films of carbon nanotubes," Nat. Nanotechnol. **6**, 788–792 (2011).
14. Y. Wang, L. Wang, T. Yang, X. Li, X. Zang, M. Zhu, K. Wang, D. Wu, and H. Zhu, "Wearable and highly sensitive graphene strain sensors for human motion monitoring," Adv. Funct. Mater. **24**, 4666–4670 (2014).
15. A. K. Geim and K. S. Novoselov, "The rise of graphene," Nat. Mater. **6**, 183–191 (2007).
16. D. Wei, Y. Liu, Y. Wang, H. Zhang, L. Huang, and G. Yu, "Synthesis of N-doped graphene by chemical vapor deposition and its electrical properties," Nano Lett. **9**, 1752–1758 (2009).
17. R. Ivaškevičiūtė-Povilauskienė, L. Minkevičius, D. Jokubauskis, A. Urbanowicz, S. Indrišiūnas, and G. Valušis, "Flexible materials for terahertz optics: advantages of graphite-based structures," Opt. Mater. Express **9**, 4438–4446 (2019).
18. J. Lin, Z. Peng, Y. Liu, F. Ruiz-Zepeda, R. Ye, E. L. G. Samuel, M. J. Yacaman, B. I. Yakobson, and J. M. Tour, "Laser-induced porous graphene films from commercial polymers," Nat. Commun. **5**, 5714 (2014).
19. M. G. Stanford, K. Yang, Y. Chyan, C. Kittrell, and J. M. Tour, "Laser-induced graphene for flexible and embeddable gas sensors," ACS Nano **13**, 3474–3482 (2019).
20. I. Karakurt, J. Elwood, X. Li, L. Beker, E. Sweet, W. Cai, and L. Lin, "Membraneless microfluidic redox battery for wearable electronics applications," in *19th International Conference on Solid-State Sensors, Actuators and Microsystems* (IEEE, 2017), pp. 1820–1823.
21. M. Ren, J. Zhang, and J. M. Tour, "Laser-induced graphene hybrid catalysts for rechargeable Zn-air batteries," ACS Appl. Energy Mater. **2**, 1460–1468 (2019).
22. L. Li, J. Zhang, Z. Peng, Y. Li, C. Gao, Y. Ji, R. Ye, N. D. Kim, Q. Zhong, Y. Yang, H. Fei, G. Ruan, and J. M. Tour, "High-performance pseudocapacitive microsupercapacitors from laser-induced graphene," Adv. Mater. **28**, 838–845 (2016).
23. W. Song, J. Zhu, B. Gan, S. Zhao, H. Wang, C. Li, and J. Wang, "Flexible, stretchable, and transparent planar microsupercapacitors based on 3D porous laser-induced graphene," Small **14**, 1702249 (2018).
24. C. Zhang, Z. Peng, C. Huang, B. Zhang, C. Xing, H. Chen, H. Cheng, J. Wang, and S. Tang, "High-energy all-in-one stretchable microsupercapacitor arrays based on 3D laser-induced graphene foams decorated with mesoporous ZnP nanosheets for self-powered stretchable systems," Nano Energy **81**, 105609 (2021).
25. Z. Wang, G. Wang, W. Liu, B. Hu, J. Liu, and Y. Zhang, "Patterned laser-induced graphene for terahertz wave modulation," J. Opt. Soc. Am. B **37**, 546–551 (2020).
26. M. S. Masyukov and A. N. Grebenchukov, "Temporally modulated metamaterial based on a multilayer graphene structure," Phys. Rev. B **104**, 165308 (2021).